ORIGINAL ARTICLE

Journal of Anatomy

ANATOMICAL SOCIETY WILEY

A spatial–temporal map of glutamatergic neurogenesis in the murine embryonic cerebellar nuclei uncovers a high degree of cellular heterogeneity

Filippo Casoni[1,2] [iD] | **Laura Croci**[1] | **Francesca Marroni**[1,2] | **Giulia Demenego**[1,2] | **Chiara Marullo**[1] | **Ottavio Cremona**[1,2] | **Franca Codazzi**[1,2] | **G. Giacomo Consalez**[1,2]

[1]Division of Neuroscience, IRCCS San Raffaele Scientific Institute, Milan, Italy

[2]Vita-Salute San Raffaele University, Milan, Italy

Correspondence
Filippo Casoni,
IRCCS San Raffaele Scientific Institute and Vita-Salute San Raffaele University, Milan, Italy.
Email: casoni.filippo@hsr.it

Abstract

The nuclei are the main output structures of the cerebellum. Each and every cerebellar cortical computation reaches several areas of the brain by means of cerebellar nuclei processing and integration. Nevertheless, our knowledge of these structures is still limited compared to the cerebellar cortex. Here, we present a mouse genetic inducible fate-mapping study characterizing rhombic lip-derived glutamatergic neurons of the nuclei, the most conspicuous family of long-range cerebellar efferent neurons. Glutamatergic neurons mainly occupy dorsal and lateral territories of the lateral and interposed nuclei, as well as the entire medial nucleus. In mice, they are born starting from about embryonic day 9.5, with a peak between 10.5 and 12.5, and invade the nuclei with a lateral-to-medial progression. While some markers label a heterogeneous population of neurons sharing a common location (BRN2), others appear to be lineage specific (TBR1, LMX1a, and MEIS2). A comparative analysis of TBR1 and LMX1a distributions reveals an incomplete overlap in their expression domains, in keeping with the existence of separate efferent subpopulations. Finally, some tagged glutamatergic progenitors are not labeled by any of the markers used in this study, disclosing further complexity. Taken together, our results obtained in late embryonic nuclei shed light on the heterogeneity of the excitatory neuron pool, underlying the diversity in connectivity and functions of this largely unexplored cerebellar territory. Our findings contribute to laying the groundwork for a comprehensive functional analysis of nuclear neuron subpopulations.

KEYWORDS
cerebellar nuclei, cerebellum, genetic inducible fate mapping, glutamatergic projection neurons, neurogenesis

Filippo Casoni and Laura Croci contributed equally.

1 | INTRODUCTION

The function of the cerebellum requires an interplay between its cortex and output circuitry, represented almost entirely by the cerebellar nuclei (CN). A broad range of inputs from the entire central nervous system is elaborated by the cerebellar cortex (Kebschull et al., 2023) and forwarded to the CN, which projects their output mainly to the brainstem and diencephalon.

In both mice and humans, the CN consist of a heterogeneous collection of neurons positioned deep within the cerebellar hemispheres. Although there are differences in size and complexity between the mouse and human CN, the general organization and function are well conserved across mammalian species. The human CN comprise four separate nuclei named fastigial, globose, emboliform, and dentate, from medial to lateral (Kebschull et al., 2023; Weidenreich, 1899). Instead, rodent cerebella contain three separate nuclei, since the globose and emboliform nuclei are anatomically fused, giving rise to the so-called interposed nucleus. Thus, from medial to lateral, the rodent CN consist of the medial (MED), interposed (INT), and lateral (LAT) (Korneliussen, 1968, Paxinos, 2007).

It is now evident that the individual nuclei can be further subdivided into various subnuclei, which might reflect the modular organization of the olivo-cortico-nuclear system (Apps et al., 2018; Apps & Hawkes, 2009). Each of these subnuclei plays its own role and has its set of connections, although it remains largely unknown how these subnuclei exert their function, as the classification of neuronal types making up the CN subnuclei is still in progress. Two or three classes of CN neurons were historically described merely based on their soma sizes (Goodman et al., 1963; Korneliussen, 1968; Lugaro, 1895) and the synthesis and release of glutamate or GABA (Ankri et al., 2015; Bagnall et al., 2009; Houck & Person, 2015; Uusisaari & Knopfel, 2008, 2010).

Recently, CN neurons were subdivided into five classes (reviewed in Kebschull et al., 2023). This classification was based on different lines of evidence including neurotransmitter production, morphology, location, and transcriptomic signatures identified in adult mice. According to this subdivision, the CN contain two types of glutamatergic projection neurons, referred to as class A and class B, which exhibit different morphological features and transcriptomic signatures (Kebschull et al., 2020, 2023). Additionally, three classes of GABAergic or GABA- and glycinergic neurons were identified, differing with respect to physiology and developmental origin (Kebschull et al., 2020; Uusisaari & Knopfel, 2010, 2011).

A robust link between CN neuron progenitors and their mature counterparts is still missing or is largely incomplete. Significant progress has been made through the discovery in mouse embryos of molecular cues controlling glutamatergic neurogenesis, in particular the development of glutamatergic neurons populating the CN, through the use of *atonal basic helix–loop–helix transcription factor 1* (*Atoh1*)-tagged mouse cerebella. On the one hand, transgenic mice were generated where *Atoh1*-positive precursors and their derivatives were irreversibly tagged by an inducible Cre recombinase upon tamoxifen administration at different consecutive time points. This enabled discrete cellular cohorts to be identified at specific time windows (Machold & Fishell, 2005). In parallel, a similar analysis was conducted in a transgenic line in which the *Atoh1* promoter drove beta-galactosidase expression (Wang et al., 2005), resulting in comparable conclusions. These studies established the notion that *Atoh1*+ rhombic-lip (RL) derivatives include not only cerebellar granule cells (GCs), the precerebellar nuclei projecting mossy fibers to them, and several proprioceptive nuclei but also the CN. Moreover, a more recent study demonstrated that, in the mouse, lateral nuclei develop thanks to *Lhx9* gene expression in the nuclear transitory zone (NTZ), which is subsequently downregulated upon induction of *Tbr1* transcription (Green & Wingate, 2014). Early downregulation of *Lhx9* in the avian cerebellum likely accounts for the evolutionarily recent appearance of the LAT (Green & Wingate, 2014).

CN precursors migrate out of the RL as part of the so-called rostral RL migratory stream, tangentially along the pial surface of the cerebellar primordium (Wang et al., 2005). In chick embryos, glutamatergic cerebellar progenitors are sensitive to time-dependent migratory cues. Early-born cells have a single long leading process that guides their migration toward the midline, whereas later-born GCs precursors, which also migrate ventrally, lose their sensitivity to netrin1 and upregulate *Robo2*. This causes them to halt at the lateral edge of the cerebellar primordium in response to SLIT2 expressed at the rhombic lip and ventral midline (Gilthorpe et al., 2002).

In the mouse, CN precursors reach the NTZ as early as E11.5 (Machold & Fishell, 2005; Wang et al., 2005). While migrating, neurons downregulate *Atoh1* and upregulate several transcription factors, including PAX6 (E13.5) (Fink et al., 2006) and POU3F1 (E10.5) (Wu et al., 2022). In the NTZ, the nascent CN express TBR2 and TBR1 (Fink et al., 2006), which mark a subset of neurons of the MED, as well as BRN2 (POU3F2), OLIG2, and/or IRX3, which label mainly LAT and/or INT neuronal subsets (Wu et al., 2022).

The present genetic inducible fate-mapping (GIFM) study expands the analysis of progenitors derived from the *Atoh1*+ lineage and describes the distribution of molecularly defined derivatives of this lineage in the perinatal and adult CN. Our GIFM results and the availability of the *Atoh1::CreER^{T2}* line will facilitate the dissection of developmental trajectories that link embryonic and adult excitatory lineages in the CN.

2 | MATERIALS AND METHODS

2.1 | Animal care

All experiments described here were performed in agreement with the stipulations of the San Raffaele Scientific Institute Animal Care and Use Committee (I.A.C.U.C.).

2.2 | Mouse genetics

2.2.1 | Atoh1::CreER^{T2}/0 mouse line

The *Atoh1::CreER^{T2}/0* mouse line was provided from the Jackson Laboratory (Tg(Atoh1-Cre/Esr1*)14Fsh/J, Stock No: 007684; RRID:IMSR_JAX:007684). These transgenic mice express a tamoxifen-inducible Cre recombinase (CreER^{T2}) driven by the *Drosophila atonal* promoter. Upon tamoxifen (TAM) induction, this fusion protein becomes active in neural progenitors of the cerebellar rhombic lip and dorsal hindbrain (Machold & Fishell, 2005, https://www.jax.org/strain/007684). For genotyping: DNA was extracted from the tail of embryos or mice at P12 using Xpert directXtract Lysis Buffer Kit (Grisp Research Solutions, Biocell), and the analysis was carried out using the following PCR primers to test the presence of *Atoh1::CreER^{T2}* transgene:

-oIMR1084 (Forward): 5′ GCG GTC TGG CAG TAA AAA CTA TC 3′.

-oIMR1085 (Reverse): 5′ GTG AAA CAG CAT TGC TGT CAC TT 3′.

The amplification product is verified through an agarose gel (1,5% in TAE 1X) electrophoresis. The expected band is 100 bp for *Atoh1::CreER^{T2}/0*.

2.2.2 | Rosa26tdTomato/+ mouse line

The Rosa26tdTomato is a congenic mouse line on C57BL/6J background and was provided by the Jackson Laboratory (B6. Cg-Gt(ROSA)26sor Tm14(CAG-tdTomato)Hze/J, Stock #007914; RRID:IMSR_JAX:007914). This strain contains a floxed STOP cassette preventing the CAG promoter-driven transcription of a coding sequence encoding the red fluorescent protein (RFP) variant (tdTomato) inserted into the Gt(ROSA)26Sor locus. After Cre-mediated recombination, this strain expresses robust tdTomato fluorescence.

2.2.3 | Mouse lines crossing

In this project, all the experiments were performed on embryos obtained by crossing *Atoh1::CreER^{T2}/0* and *Rosa26$^{tdT/+}$* mice.

2.2.4 | Tamoxifen administration

Tamoxifen (Sigma-Aldrich, T5648) was dissolved in corn oil (Sigma-Aldrich, C8267) at a concentration of 10 mg/mL by o/n shaking at 37°. Tamoxifen (approximately 80 mg/kg mouse body weight) was delivered by oral gavage to pregnant dams at specific days of embryonic development. In case of experiments on adult mice, pups were delivered by cesarean section at E18.5 and given to a foster mother.

2.3 | Tissue preparation and processing

Embryos were fixed for 6–8 h by immersion with 4% PFA in 1× PBS. Mice were anesthetized using Avertin (Sigma) and perfused with 0.9% NaCl followed by 4% PFA in 1× PBS. The tissues were cryoprotected overnight in 30% sucrose, 1× PBS, and embedded in a 3:1 solution of embedding medium OCT (Bioptica) and 30% sucrose, then stored at −80°C. For immunofluorescence staining, 14-µm-thick sagittal or rostral sections were cut using a Leica cryotome.

2.4 | Immunofluorescence staining

Immunofluorescence was performed as described previously (Badaloni et al., 2019; Casoni et al., 2017, 2020). Briefly, sections were washed in 1× PBS to remove OCT and, if necessary, antigen retrieval was performed by heating sections in a 10 mM citrate solution, pH 6, in a microwave for 5′. Sections were blocked/permeabilized in 10% goat serum, and 0.3% Triton X-100 in 1× PBS for 1 h, and then incubated with primary antibodies overnight at 4°C. After three washing in 1× PBS, sections were incubated with secondary antibodies (1:500, Molecular Probes Alexa Fluor, Life Technologies) at room temperature for 2 h, washed three times in 1× PBS, counterstained with 4′,6-diamidino-2-phenylindole (DAPI, Sigma, 1:2000 in 1× PBS) for 5′, and mounted with fluorescent mounting medium (Dako). The LMX1A antibody detection capability was improved using the Tyramide Signal Amplification kit (TSA, Perkin Elmer), in accordance with manufacturer's instructions.

2.5 | Antibodies

BRN2, rabbit, 1:500, Cell Signaling, catalog number 12137, RRID:AB_2797827, requires antigen unmasking; LMX1a, rabbit, 1:3000, Millipore, catalog number AB10533, RRID:AB_10805970, requires antigen unmasking and TSA; mCherry, chicken, 1:500, Novus Biologicals, catalog number NBP2-25158, RRID:AB_2636881; TBR1, rabbit, 1:3000 Abcam, catalog number Ab31940, RRID:AB_2200219, requires antigen unmasking; TBR1, mouse, 1:100, Proteintech, catalog number 66564-1-Ig, RRID:AB_2881925, requires antigen unmasking; MEIS2, mouse, 1:400, Santa Cruz Biotechnology, catalog number sc-515470 RRID: AB_3076386.

2.6 | Microscopy and image processing

2.6.1 | Fluorescence microscopy

Optical microscopy was carried out using a Mavig RS-G4 confocal microscope with 20x magnification. Quantitative and morphometric

FIGURE 1 Atoh1 lineage progenitors migrate into the embryonic CN from TamE9.5 to TamE12.5, in a lateral-to-medial progression. The perimeters of cerebella and each CN are delimited by white dashed and red dotted lines, respectively. (a–e) Anti-tdT immunofluorescence in rostral hemisections of E18.5 cerebella. *Atoh1* lineage neurons are visible in the CN from TamE9.5 to TamE12.5. Only a small number of TamE9.5 neurons of the early-born cohort are detected (a) and mostly occupy the dorsolateral area of the LAT. TamE10.5 (b) and TamE11.5 (c) tdT+ neurons occupy the dorsolateral portion of the LAT, and the dorsomedial area of the INT and the MED. Solid line box in (b) shows small and large glutamatergic neurons (arrowheads and arrows, respectively). TamE12.5 tdT+ neurons (d) are visible in the medial area of the INT and the entire MED, while only few neurons occupy the lateral area of the LAT. TamE13.5 tdT+ neurons (e) are not visible in the CN. (a′–e′) Anti-tdT immunofluorescence in caudal hemisections of E18.5 cerebella. *Atoh1* lineage neurons are visible in the CN (dotted red lines) from TamE9.5 to TamE12.5. Only sparse neurons occupy the CN in the caudal region of the TamE9.5 cerebellum (a′). TamE10.5 (b′) and TamE11.5 (c′) tdT+ neurons are visible in the MED, INT, and LAT. TamE12.5 tdT+ neurons (d′) are mostly present in the medial area of the INT and the MED. Virtually no TamE13.5 tdT+ neurons (e′) are present in the CN. Solid red arrowheads in (e, e′) point to GC progenitors in the external granular layer. Size bar in (a): 200 μm.

evaluations were performed with the ImageJ software (https://imagej.net/software/fiji/, RRID:SCR_003070) using the selection tool to delimit areas of interest. Digital images were processed with Adobe Photoshop (https://www.adobe.com/products/photoshop.html RRID:SCR_014199) to adjust contrast and brightness and to create cartoons in Figures 4 and 6.

The data that support the findings of this study are openly available in Allen Brain Atlas at https://developingmouse.brain-map.org/ (Allen-Institute-for-Brain-Science, 2009).

2.7 | Data sharing

A previous version of this article is published on Biorxiv, https://www.biorxiv.org/content/10.1101/2023.10.22.563467v1.

3 | RESULTS

To investigate the cellular composition of the mouse CN, we utilized a tamoxifen (Tam)-inducible *Atoh1::CreER*[T2]/0 transgenic mouse line (Machold & Fishell, 2005; Wingate, 2005) mated with a robust Cre-inducible *tdTomato* (tdT) reporter line (Madisen et al., 2010). *Atoh1* is expressed in the rhombic lip and is essential for the development of glutamatergic neurons of the cerebellum (Machold & Fishell, 2005; Wang et al., 2005).

GIFM (reviewed in Legue & Joyner, 2010) allows temporal control of Cre-mediated recombination for a ~24 h time window subsequent to Tam injection. Tam (70 mg/kg) was administered via oral gavage to pregnant dams at E9.5, E10.5, E11.5, E12.5, or E13.5. In this paper, cerebella were analyzed at E18.5 and P45.

3.1 | Distribution of glutamatergic lineage neurons in the late embryonic CN

Upon Tam administration at E9.5 and immunofluorescence analysis at E18.5 (hereon TamE9.5), we only observed tdT fluorescence in a small number of cells restricted to the dorsal area of the presumptive LAT and INT CN (see red dotted lines), in rostral sections (Figure 1a), while hardly any cells were tagged in caudal sections (Figure 1a′).

In rostral sections, Tam administration at E10.5 and E11.5 reveals robust tagging in the dorsal and lateral area of the LAT, in the dorsal and medial area of the INT, and throughout the MED (Figure 1b,c). In caudal sections, we observed tdT+ cells in the medial portion of the INT after TamE10.5 and throughout the INT after TamE11.5; moreover, diffused signal is observed in the caudal MED (Figure 1b′,c′).

In TamE12.5 rostral sections, tdT+ cell numbers dropped in the dorsal portion of the LAT compared to previous stages of Tam induction: in fact, only few tdT+ cells were tagged in the lateral portion of the LAT. Robust tdT tagging was observed in the dorsomedial portion of the INT, and throughout the MED (Figure 1d). Tam administration at E12.5 also revealed very few tagged neurons in the caudal INT, while numerous cells were tdT+ in the caudal MED (Figure 1d′).

Finally, in TamE13.5 cerebella, hardly any cells were tagged in rostral or caudal sections of the CN, (Figure 1e,e′). As expected, numerous cells populating the external granular layer were positive for tdTomato at this stage (Figure 1e,e′ red arrowhead).

At all developmental stages examined, we observed a mixed population of *Atoh1*-tagged glutamatergic neurons, containing both large (white arrows in the inset of Figure 1b) and small cells (white arrowheads in the inset of Figure 1b), in keeping with observations made in the adult CN (Kebschull et al., 2020; Uusisaari & Knopfel, 2011).

Our data indicate that *Atoh1*-tagged glutamatergic neurons occupy the dorsolateral and dorsomedial areas of the LAT and INT, respectively, at rostral levels of the CN. The MED, occupied by later-born neurons, displays Atoh1-tagged glutamatergic neurons both in rostral and caudal sections. In all nuclei, at E18.5, ventral territories are occupied predominantly by non-glutamatergic neurons (unpublished data).

We further investigated the distribution of the *Atoh1*-tagged glutamatergic neurons in adult rostral sections. Rostrally, the LAT displayed more cells in the TamE10.5 section (Figure 2a,a′ dashed cyan lines) compared to TamE11.5 and TamE12.5 sections (Figure 2b–c′ dashed cyan lines). Caudally, fewer cells are visible in the MED of TamE10.5 and TamE11.5 sections (Figure 2d–e′ dashed cyan lines) compared to TamE12.5 sections (Figure 2f,f′ dotted cyan line).
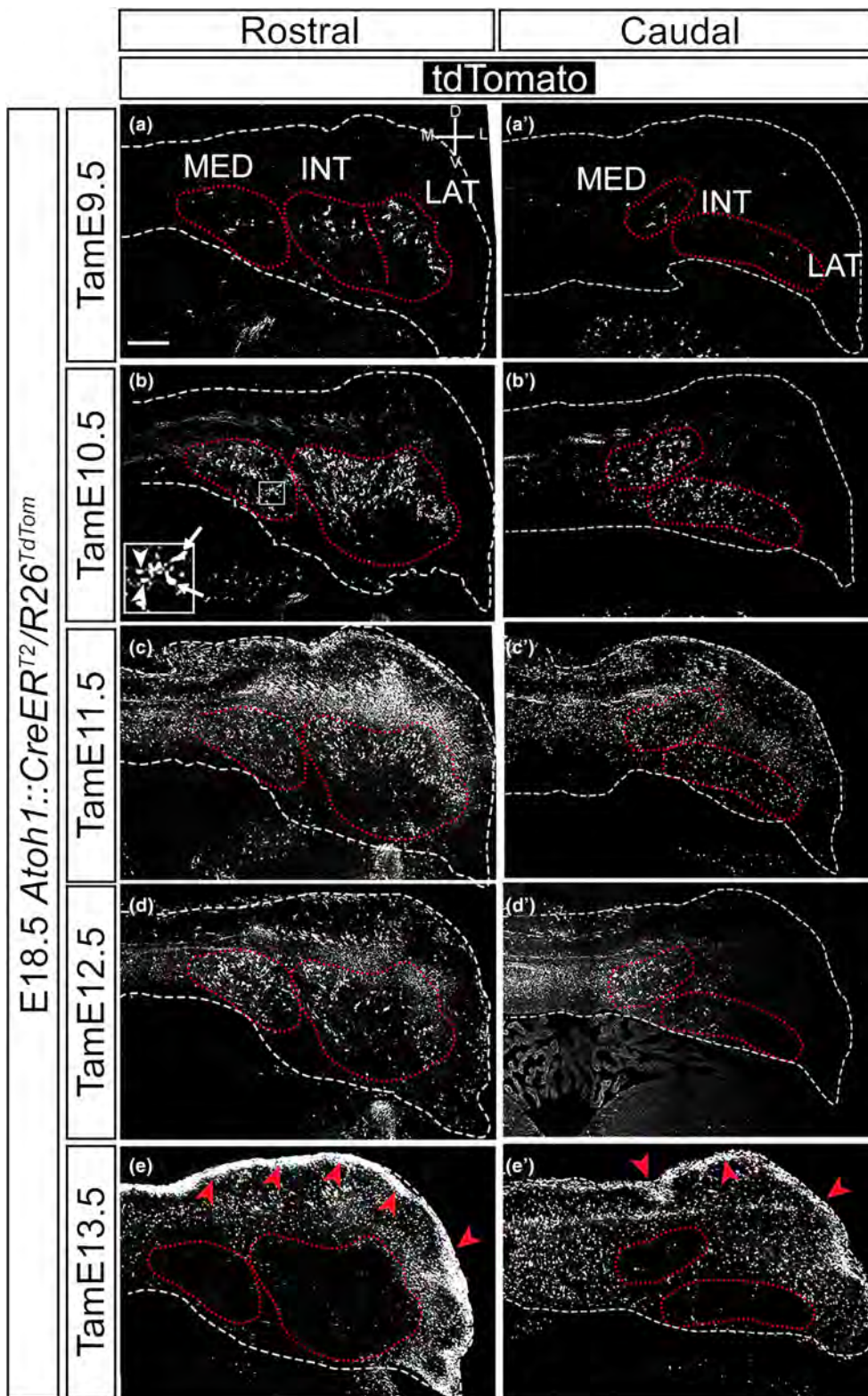
3.2 | BRN2 labels a heterogeneous early-born population of LAT and INT neurons

To further characterize CN development, we employed established markers of different CN components. Antibodies for BRN2, a POU-domain transcription factor (He et al., 1989), label the LAT and INT (not the MED) during late gestation embryogenesis (Fink et al., 2006). We performed dual immunofluorescence for BRN2 and tdT at E18.5 on cerebellar sections from litters treated with Tam at different embryonic stages.

BRN2+ cells form compact cellular aggregates throughout the LAT and INT of rostral cerebellar sections. Our data demonstrate that tdT+/BRN2+ cells localize rostrally in the dorsomedial area of the INT and the dorsolateral and ventrolateral territory of the LAT
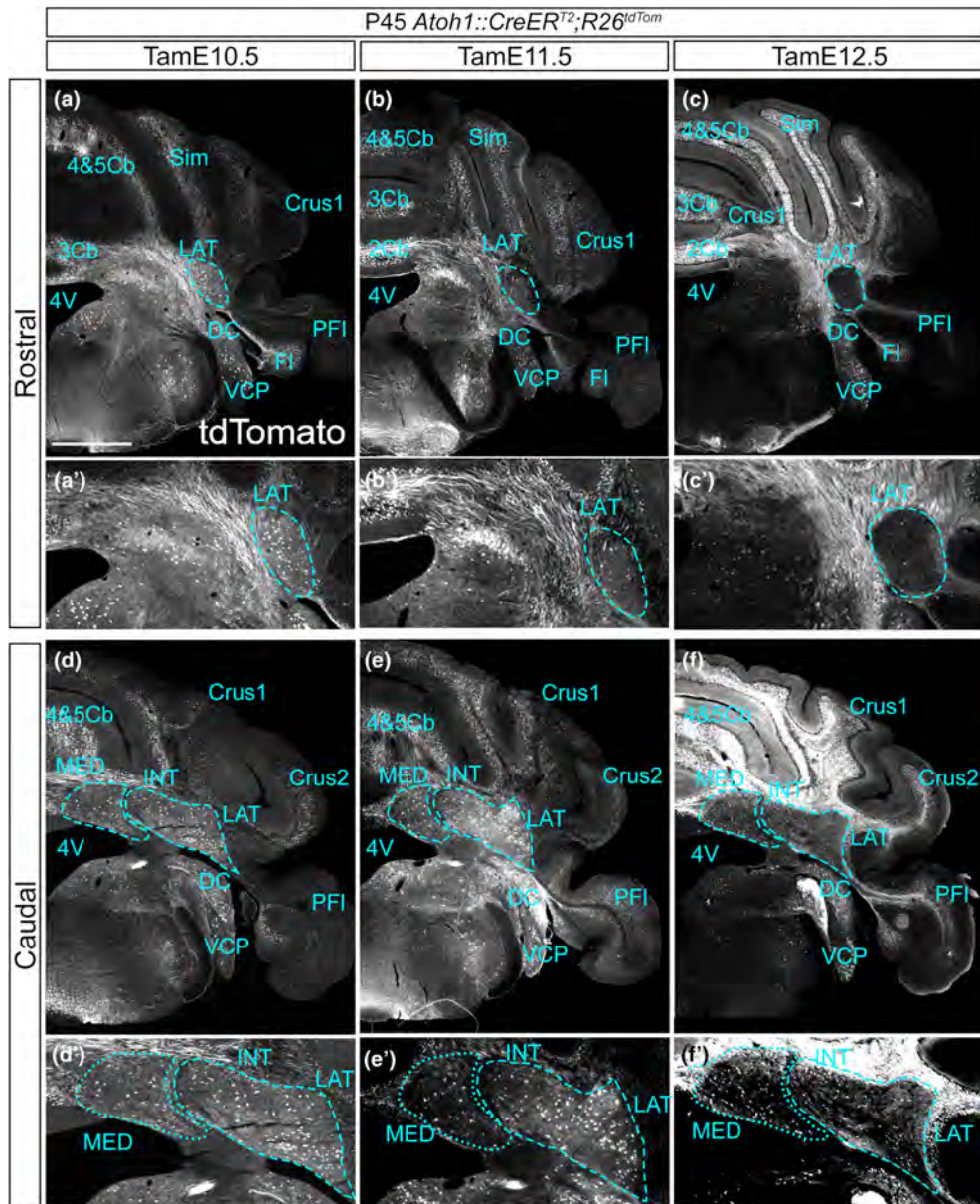
FIGURE 2 The distribution of *Atoh1* lineage cells in the adult reflects the lateral to medial progression observed in late embryonic sections. The perimeter of each CN is delimited by dashed lines. Immunostaining against tdT in *Atoh1::CreER^T2/Rosa26^tdT* adult (P45) rostral cerebellar hemisections shows recombination in the LAT (cyan dashed lines); (a–c) (magnification in a′–c′). In rostral sections, anti-tdT staining reveals *Atoh1* lineage neurons in the LAT (cyan dashed lines) from TamE10.5 to TamE12.5. The number of tdT-tagged cells in the LAT decreases from TamE10.5 (a, a′) to TamE12.5 (c, c′). In caudal sections (d–f, magnification in d′–f′), anti-tdT staining shows *Atoh1* lineage neurons in the LAT, INT, and MED (cyan dashed lines). From TamE10.5 (d, d′) to TamE12.5 (f, f′), the number of cells decreases in the LAT and progressively increases in the MED. Crus1, Crus 1 of the ansiform lobule; Crus2, Crus 2 of the ansiform lobule; DC, dorsal cochlear nucleus; FI, flocculus; Int, interposed nucleus; Lat, lateral nucleus; Med, medial nucleus; PFI, paraflocculus; Sim, simple lobule; VCP, Ventral cochlear posterior nucleus; 3Cb, cerebellar lobule III; 4&5Cb, cerebellar lobules IV and V. Size bar in (a): 1 mm.

(Figures 3a–d and 6a). Moreover, our results suggest that BRN2 is an early-born temporal cohort (Figures 3b and 6a) peaking at E10.5. Only few tdT+/BRN2+ neurons localize in the caudal MED (Figures 3b′ and 6a). Hardly any colocalization was found in TamE11.5 and TamE12.5 caudal sections. Interestingly, many tdT+ cells tagged at E11.5 were negative for BRN2, indicating that this protein is not an exhaustive marker of glutamatergic CN neurons (Figure 3c′,d′, both boxes). Finally, no double-positive cells were found in E18.5-TamE13.5, either at rostral or at caudal locations (not shown).

3.3 | MEIS2 labels a later-born population of excitatory neurons

Meis2 belongs to a family of Pbx-related homeobox genes (Nakamura et al., 1996) and is distributed in all three CN (Morales & Hatten, 2006; Willett et al., 2019). Using antibodies specific for MEIS2 and tdT at different stages of Tam induction, we showed that tdT+/MEIS2+ cells localize rostrally in the dorsal INT and in the lateral area of the LAT (Figures 3e–g and 6b), while in the caudal
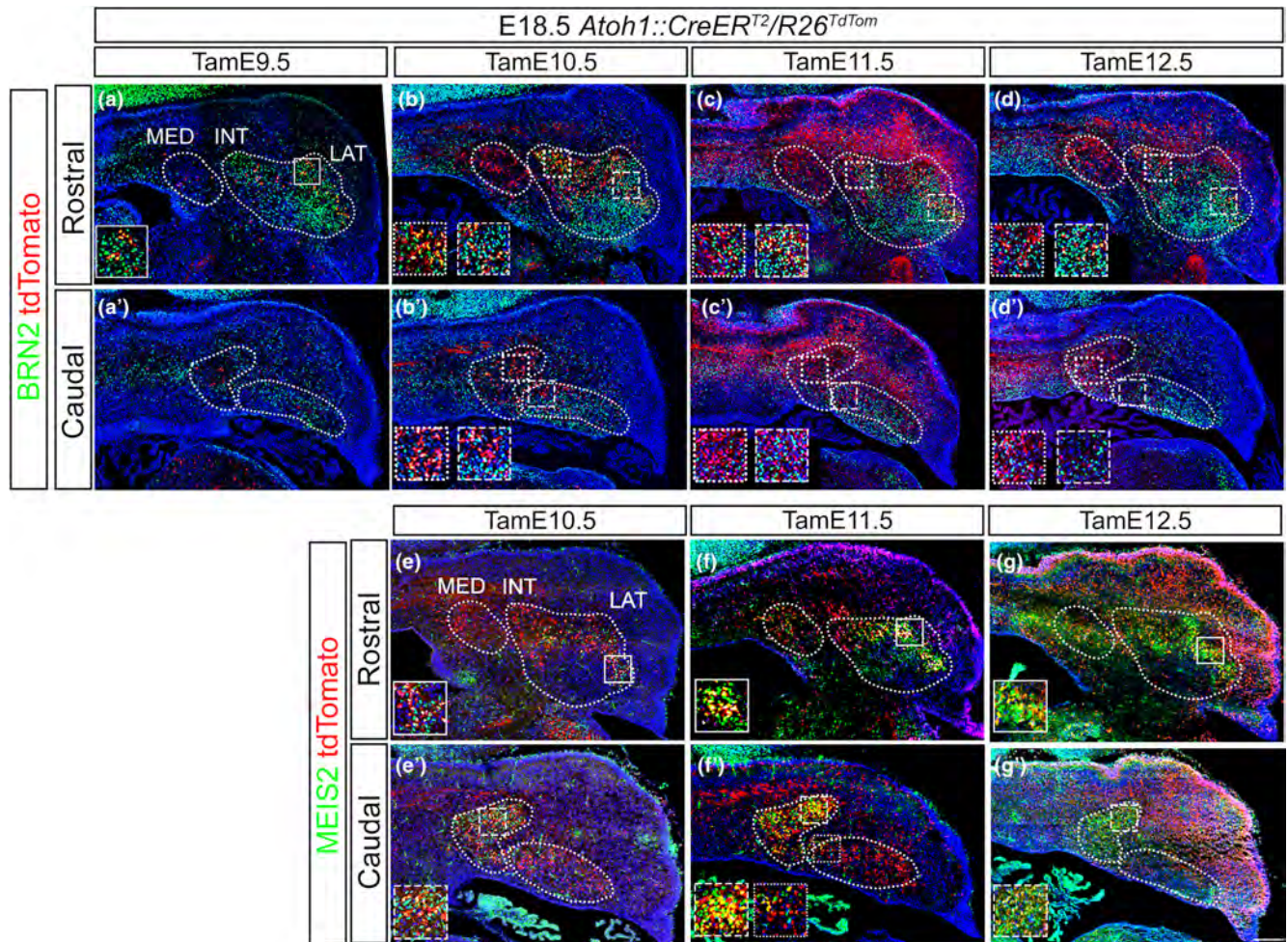
FIGURE 3 *Atoh1*-lineage glutamatergic neurons express BRN2 and MEIS2 in selective territories of the cerebellar nuclei. (a–d) Anti-tdT and BRN2 double immunofluorescence in rostral hemisections of E18.5 cerebella. BRN2+ cells form compact cellular clusters throughout the LAT and INT. Sparse TamE9.5 tdT+ neurons are also positive for BRN2 in the LAT (solid line box, in a) and INT (a). Most of the TamE10.5 tdT+ neurons are BRN2+ in the dorsolateral area of the LAT (dashed box in b) and in the dorsal area of the INT (dotted box in b). TamE11.5 and TamE12.5 tdT+ neurons are also BRN2+ in the lateral portion of the LAT (dashed boxes in c, d) and dorsomedial portion of the INT (dotted boxes in c, d). (a′–d′) Anti-tdT and BRN2 double immunofluorescence in caudal hemisections of E18.5 cerebella. Virtually, no tdT+ cells are present in TamE9.5 caudal sections (a′). Only sparse cells are double positive in the MED and INT in TamE10.5 sections (b′, dotted and dashed boxes, respectively). Nearly all tdT+ cells tagged at E11.5 and E12.5 are negative for BRN2 (boxes in c′ and d′). (e–g) Anti-tdT and MEIS2 double immunofluorescence in rostral hemisections of E18.5 cerebella. Few MEIS2, tdT double-positive cells are visible in the lateral area of the LAT and INT in TamE10.5 sections (solid box in e). The bulk of MEIS2+ neurons are tagged at E11.5 in the dorsomedial and in the lateral area of the LAT and the dorsolateral area of the INT (solid box in f). MEIS2+ neurons tagged at E12.5 are found in the LAT (solid box in g) and the INT. (e′–g′) Anti-tdT and MEIS2+ double immunofluorescence in caudal hemisections of E18.5 cerebella. Most of the MEIS2+ are TdT+ in the MED (dashed boxes in e′, f′, g′) both in the middle portion and in the DLP. Size bar in (g′): 200 μm.

sections of the cerebellum, tdT+/MEIS2+ cells are found in the MED (Figures 3e′–g′ and 6b). Our data suggest that the MEIS2 cohort is generated later than BRN2+ cells (Figures 3f,f′ and 6b), with a peak at E11.5.

3.4 | TBR1 and LMX1a mark two partially overlapping subpopulations of glutamatergic neurons of the MED

We performed TBR1 and tdT immunostainings on E18.5 cerebellar rostral sections. Irrespective of the stage of Tam induction, we only observed double labeling in the MED (Figure 4a–d). Anatomically, adult medial nuclei comprise a rostral part, a caudal part, and a dorsolateral protuberance (DLP) (Fujita et al., 2010, 2020; Korneliussen, 1968). Accordingly, in the E18.5 MED, we identified a ventrolateral mass (VL), a middle mass (M), and a DLP that is only visible in caudal sections (reviewed in Kebschull et al., 2023); (sketched in Figure 4e). Most of the tdT+/TBR1+ cells were found in the ventrolateral area of the MED in rostral sections, mostly at TamE11.5 and TamE12.5 (Figures 4b,c and 6c). In caudal sections, double-positive cells were found in the ventrolateral and middle portion of the MED, and only a small number in the DLP (Figures 4b′,c′ and 6c). Taken together, these data demonstrate that most of the
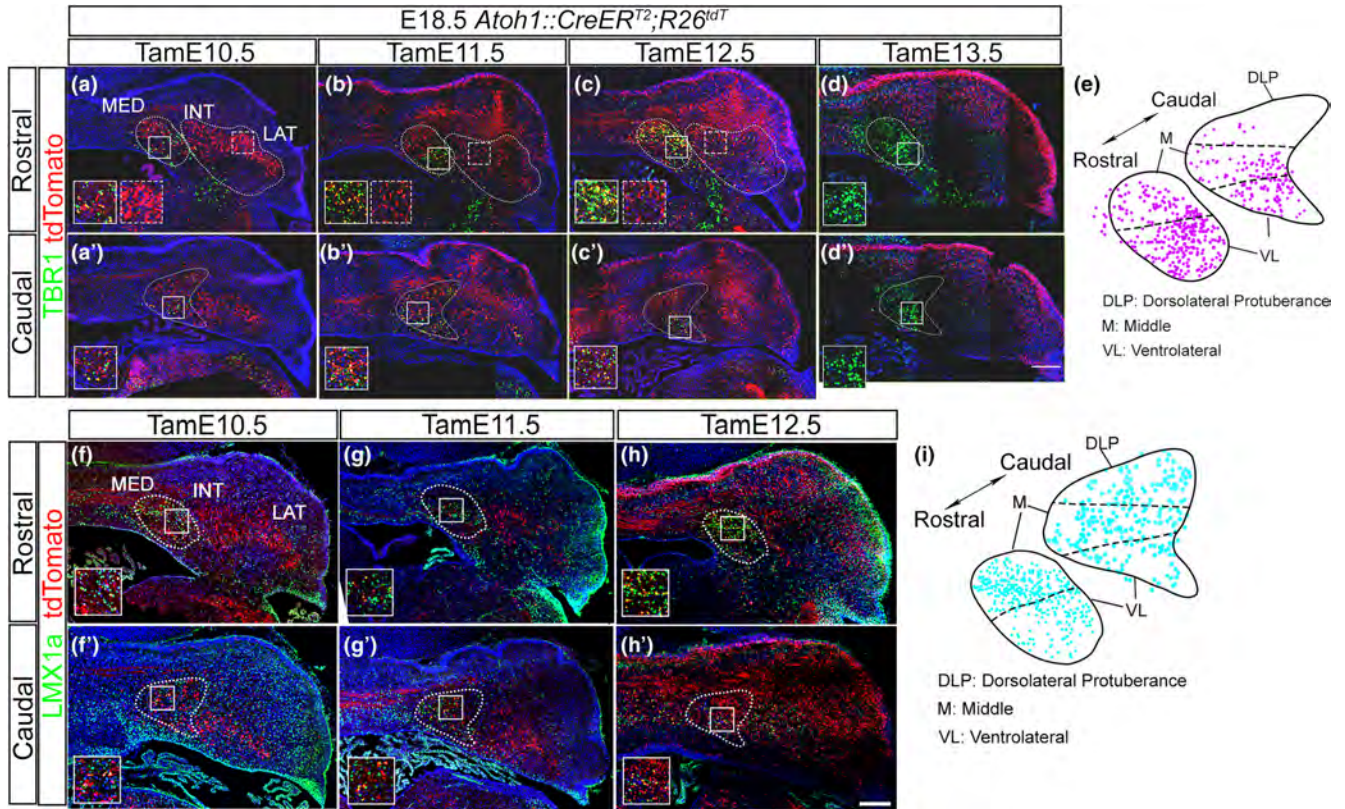
FIGURE 4 TBR1+ and LMX1a+ glutamatergic neurons overlap only partially in the MED. The perimeter of each CN is delimited by dotted lines. (a–d') All sections (E18.5) were immunostained for tdT (red) and TBR (green). (a–d) In rostral sections, TBR1+ cells are located in the ventrolateral and middle area of the MED (solid line boxes). No TBR1+ cells can be found in the INT or LAT (dashed line boxes). (a'–d') In caudal sections, TBR1+ neurons are localized in the ventrolateral and middle areas of the MED (solid line boxes). (e) Graphical representation of rostral and caudal sections of the MED: Individual TBR1+ neurons shown in (a–d') are mapped. The map confirms the presence of TBR1+ cells in the ventrolateral and middle area of the MED, and their near absence in the DLP. (f–h') All sections (E18.5) were immunostained for tdT (red) and LMX1a (green). (f–h) In rostral sections, LMX1a+ cells localize preferentially in the middle area of the MED (solid line boxes). (f'–h') In caudal sections, LMX1a immunostaining is visible throughout the MED, including the DLP (solid line boxes). (i) Graphical representation of rostral and caudal sections of the MED. Individual LMX1a+ neurons are mapped. The map confirms that LMX1a-positive cells localize mostly in the middle area and the dorsolateral protuberance of the MED. (f–h') Presumptive LMX1a+ unipolar brush cells are found outside the CN (e.g., white arrowheads in f'). Size bar in (d' and h'): 200 μm.

TBR1+ cells detectable at E18.5 are born between E11.5 and E12.5 and occupy the ventrolateral and intermediate positions of the MED (see sketch in Figure 4e).

We also performed LMX1a and tdT double immunostaining on E18.5 cerebellar sections. We observed several LMX1a+ cells in different regions of the cerebellum, including the vermis (presumptive UBCs and granules of lobule X). In the nuclei, most of the tdT+/LMX1a+ neurons were found in the MED (Figures 4 and 6d), at both rostral (Figure 4f–h) and caudal (Figure 4f'–h') levels (Figure 6d). Anteriorly, most of the double-positive cells were tagged at E12.5 in the middle portion of the MED. In caudal sections, double-positive cells for LMX1a and tdT were found throughout the MED, including the DLP. These data indicate that the LMX1a+ cohort is generated later than the TBR1+ cohort, and that it occupies a broader area of the nucleus compared to TBR1+ cells.

These results support in prenatal sections the existence of heterogeneous populations of glutamatergic MED neurons (inter alia (Fujita et al., 2020)). To confirm this notion, we carried out a dual immunostaining of wt E18.5 cerebellar sections, using LMX1a and TBR1 antibodies (Figure 5). Our results allow the identification of three glutamatergic subpopulations of the MED: (i) LMX1a+, TBR1+; (ii) LMX1a+, TBR1–, and (iii) LMX1a–, TBR1+ (Figure 5, yellow arrowheads in 1 and 3, black arrowheads in 2 and 4, and white arrowheads in 1 and 3 respectively).

4 | DISCUSSION

The molecular mechanisms leading to the formation and organization of the cerebellar nuclei remain largely unknown. Here, we present a detailed fate-mapping analysis covering the anatomical and molecular organization of the cerebellar nuclei in space and time during embryonic development. By GIFM, we describe the molecular trajectories linking *Atoh1*+ progenitors to their molecularly defined glutamatergic derivatives in the prenatal CN. While it is difficult to establish how efficient colabeling of *Atoh1* derivatives
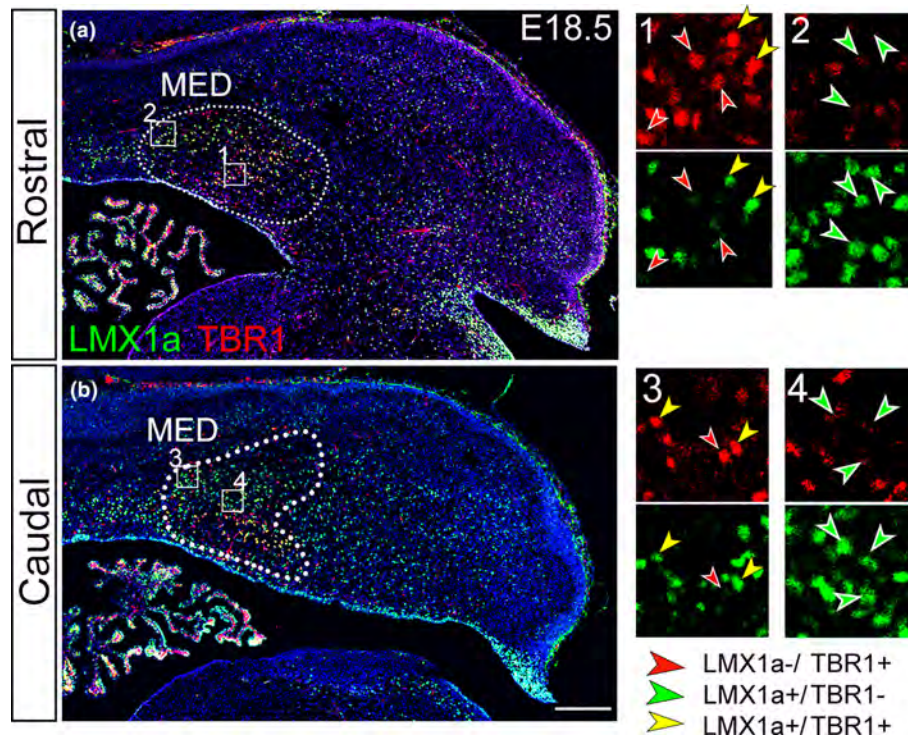
FIGURE 5 LMX1a+ and TBR1+ cell populations are only partially overlapping. (a, b) LMX1a and TBR1 immunostaining in rostral (a) and caudal (b) sections of the E18.5 MED reveals double-positive neurons, as well as cells that are only positive for either marker. LMX1a–/TBR1+ cells are displayed in boxes 1 and 3 (red arrowheads), LMX1a+/TBR1– cells are displayed in boxes 2 and 4 (green arrowheads), and LMX1a+/TBR1+ cells are displayed in boxes 1 and 3 (yellow arrowheads). Size bar in (b): 200 μm.

with markers is, due to the incomplete activation of the Cre recombinase by tamoxifen at any given stage, in this paper, we only refer to the cells that are fluorescently tagged, and make no assumptions regarding those that are not. However, in the case of BRN2, a large share of cells positive for this marker were not tagged at any induction stage, suggesting that BRN2 is not a specific marker of the *Atoh1* lineage and, consequently, it is not a glutamatergic-specific marker, in agreement with published observations (Wu et al., 2022).

4.1 | Time window and spatial progression of glutamatergic neurogenesis in the nuclei

The glutamatergic CN neuron fate is specified as *Atoh1*+ progenitors emerge from the rostral rhombic lip, migrating beneath the pial surface of the cerebellar anlage, and reach an area dubbed nuclear transitory zone (NTZ) by E14.5. While the cues promoting differential migration of GCs progenitors with respect to precerebellar progenitors have been clarified (Gilthorpe et al., 2002), not much is known about factors involved in driving CN neuronal precursors into the NTZ, from which they invade the prospective CN territory. Tamoxifen-controlled *Atoh1::CreER*^{T2} tracing shows that glutamatergic CN neurons are tagged starting at E9.5, although our data confirm prior findings indicating that the bulk of CN neurogenesis takes place between E10.5 and E12.5 (Machold & Fishell, 2005; Wang

et al., 2005). Our data reveal that CN neurogenesis proceeds from rostral to caudal (Figure 1a,a′), and from lateral to medial, with the earliest *Atoh1*+ progenitors populating the prospective LAT first. Our evidence of a lateral-to-medial progression of CN neurogenesis recapitulates findings obtained in the chick cerebellum, although a proper LAT is not present in that species (Green & Wingate, 2014; Kebschull et al., 2023).

BRN2, one marker of glutamatergic neurons, labels a large neuronal population almost exclusively located in the dorsomedial area of the INT and the dorsolateral area of the LAT (Figures 3a–d′ and 6a). However, our findings show that BRN2 also labels neurons located in ventral territories of the CN, which are never tagged by *Atoh1::CreER*^{T2}, suggesting that these cells might not be glutamatergic. Single-cell (sc-)RNAseq studies conducted in adult mouse cerebella confirm the notion that BRN2 is not a lineage-specific marker (Kebschull et al., 2020). In fact, it is also expressed by VZ-derived inhibitory precursors mostly located in the LAT and INT (Kebschull et al., 2020) (unpublished data). The dual role of BRN2 is confirmed by the fact that at E13.5, this gene colocalizes with the glutamatergic marker *Lhx9* in the NTZ (Green & Wingate, 2014; Morales & Hatten, 2006), but is also found at the same stage in the cerebellar VZ, which gives rise to inhibitory neurons (Allen-Institute-for-Brain-Science, 2009). We speculate that BRN2 may be involved in guiding migration of VZ and RL precursors away from the midline and into the INT and LAT, possibly by controlling the expression of receptors sensitive to a repulsive midline cue. At any rate, many large tdT+
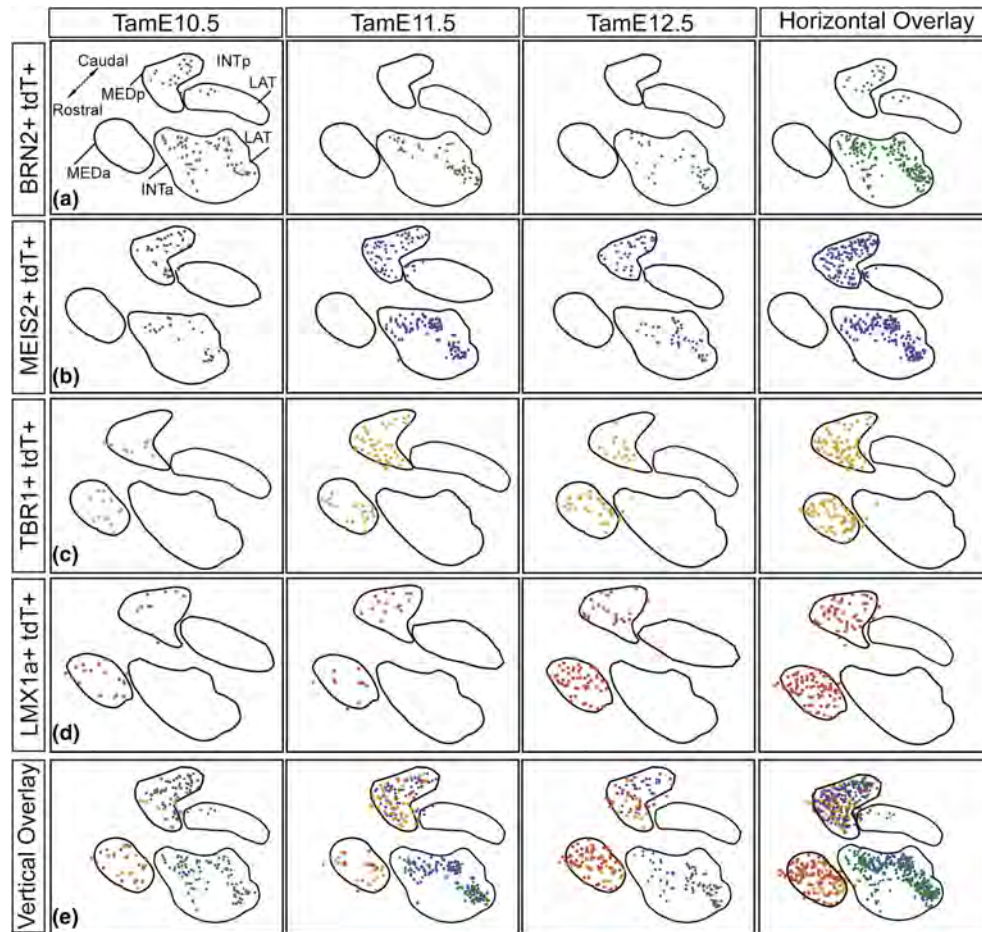
FIGURE 6 Graphic representation of the GIFM in CN neurons at different stages of Tam induction in combination with different molecular markers. The last column is the superimposition of the three stages analyzed. (a) In rostral sections, tdT+/BRN2+ neurons are located in the dorsomedial area of the INT and in the dorsolateral part of the LAT. Only a small number of double-positive neurons is visible in caudal sections of the MED. (b) In rostral sections, tdT+/MEIS2+ neurons mapped the dorsolateral area of the LAT and the dorsal area of the INT. In caudal sections, double-positive neuron cells are present across the entire MED. (c, d) tdT+/TBR1+ and tdT+/LMX1a+ neurons are visible only in the MED. (c) In caudal sections, most of the tdT+/TBR1+ cells are born between E11.5 and E12.5 and occupy the middle and ventrolateral portions of the MED. (d) In frontal sections, the bulk of tdT+/LMX1a+ cells are born at E12.5 in the medial portion of the MED, while in caudal sections, double-positive cells are found throughout the MED, including the DLP. (e) The last row represents the superimposition of all tdT+/marker+ cells for each tamoxifen induction within the CN. INTc, caudal interpositus nucleus; INTr, rostral interpositus nucleus; LATc, caudal lateral nucleus; LATr, rostral lateral nucleus; MEDc, caudal medial nucleus; MEDr, rostral medial nucleus.

cells genetically tagged were negative for BRN2, indicating that this protein is not an exhaustive marker of INT and LAT glutamatergic neurons either (e.g., Figure 3c′).

Another marker, MEIS2, labels glutamatergic precursors throughout the CN, especially in posterior territories of the MED (Figure 3e′,f′); however, many tdT+ glutamatergic precursors are MEIS2 negative in E18.5 sections. MEIS2 is a precocious marker, already expressed at robust levels in the E11.5 subpial stream (Morales & Hatten, 2006) (https://developingmouse.brain-map.org/experiment/siv?id=100077943&imageId=101289116&initImage=ish&x=6278.358960168304&y=5708.920008626071&z=5) (Allen-Institute-for-Brain-Science, 2009), likely affecting CN neuron development starting at early stages. According to a recent sc-RNAseq study, in the adult CN, MEIS2 is not expressed in GABAergic neurons in the adult CN (Kebschull et al., 2020),

confirming previous results (Morales & Hatten, 2006), while it is expressed by the majority, but not the entirety of glutamatergic excitatory neurons. Thus, the finding of tdT+ and MEIS2– neurons at birth reflects findings obtained in the adult and indicates that MEIS2+ and MEIS2– likely differ in function and/or connectivity. Moreover, MEIS2+ neuron distribution along the rostrocaudal and mediolateral axes of the CN seems discontinuous, possibly reflecting the organization of the cerebellar cortex in zones and stripes (Chung et al., 2009; Hawkes, 2018). This is in keeping with physiological data suggesting the existence of longitudinal micromodules corresponding to distinct peripheral receptive fields (Apps & Garwicz, 2005; Ekerot et al., 1991; Garwicz & Ekerot, 1994). The precise nature of adult MEIS2+ versus MEIS2– glutamatergic derivatives remains unknown to date.

4.2 | LMX1a and TBR1 label partially separate glutamatergic populations in the MED

As regards the medial nucleus, our results indicate that late embryonic glutamatergic neurons in the MED can be subdivided into TBR1;LMX1a double-positive, LMX1a+;TBR1− (or TBR1$_{weak}$), and LMX1a−;TBR1+ subpopulations. This molecular heterogeneity may contribute to the diversity of cerebellar vermis connections, both afferent and efferent. Indeed, previously published results identify five molecularly and anatomically distinct types of glutamatergic projection neurons in the adult MED, each receiving specific sets of Purkinje cells and inferior olive afferents, and projecting their output to a series of functionally related downstream targets, involved in both motor and non-motor functions (Fujita et al., 2020).

4.3 | Molecular heterogeneity of glutamatergic neurons

Globally, our findings point to a marked degree of heterogeneity in the glutamatergic progenitor pool at embryonic stages of CN development, in agreement with the existence of excitatory CN neuron subcategories in the adult nuclei (Figure 6e) (Bagnall et al., 2009; Chen & Hillman, 1993; Chung et al., 2009; Flood & Jansen, 1961; Ikeda et al., 1995). To further summarize the complexity of the glutamatergic lineage within the different CN, we generated a cartoon (Figure 6) that presents the distribution of neurons double positive for tdT and each of the markers tested. Notably, none of those markers colocalizes with tdT+ neurons localized in posterior territories of the interposed nuclei (Figures 1b′,c′ and 6e). Further studies are required to address this aspect. To complete the description of this phenotypic diversity, a higher throughput and resolution will be achievable by combining traditional morphology with the application of more recent spatial transcriptomics (Ortiz et al., 2021; Rao et al., 2021) and barcoding techniques (Kebschull & Zador, 2018). A question that emerges from our analysis and others is whether or to what extent this complexity mirrors a functional and connectomic heterogeneity, as already shown for the fastigial nucleus (inter alia, Fujita et al., 2020). The availability of Cre lines, intersectional genetics techniques (e.g., White & Sillitoe, 2017), and viral constructs for stereotaxic injection (e.g., Asemi-Rad et al., 2023), coupled with optogenetic and chemogenetic approaches (Kim et al., 2017; Nectow & Nestler, 2020), will elucidate the developmental trajectories linking embryonic and postnatal phenotypes, and allow neuronal subsets in the CN to be linked to their postsynaptic targets, exploring their function in vivo.

AUTHOR CONTRIBUTIONS

FC: Conceptualization, data curation, formal analysis, funding acquisition, investigation, resources, software, supervision, validation, writing original draft, and editing revision; LC: conceptualization, data curation, investigation, methodology, and editing original draft; FM and GD: carried out the experiment, editing original draft, and formal analysis; CM, OC, and FrC: editing original draft and investigation; GGC: conceptualization, data curation, funding acquisition, investigation, resources, supervision, validation, and editing original draft.

DATA AVAILABILITY STATEMENT

Data sharing is not applicable to this article as no new data were created or analyzed in this study.

ORCID

Filippo Casoni https://orcid.org/0000-0002-1172-8377

REFERENCES

Allen-Institute-for-Brain-Science. (2009) Allen Developing Mouse Brain Atlas [Internet].

Ankri, L., Husson, Z., Pietrajtis, K., Proville, R., Léna, C., Yarom, Y. et al. (2015) A novel inhibitory nucleo-cortical circuit controls cerebellar Golgi cell activity. *eLife*, 4, e06262.

Apps, R. & Garwicz, M. (2005) Anatomical and physiological foundations of cerebellar information processing. *Nature Reviews. Neuroscience*, 6, 297–311.

Apps, R. & Hawkes, R. (2009) Cerebellar cortical organization: a one-map hypothesis. *Nature Reviews. Neuroscience*, 10, 670–681.

Apps, R., Hawkes, R., Aoki, S., Bengtsson, F., Brown, A.M., Chen, G. et al. (2018) Cerebellar modules and their role as operational cerebellar processing units: a consensus paper [corrected]. *Cerebellum*, 17, 654–682.

Asemi-Rad, A., Ghiyamihoor, F., Consalez, G.G. & Marzban, H. (2023) Ablation of projection glutamatergic neurons in the lateral cerebellar nuclei alters motor coordination in Vglut2-Cre+ mice. *Cerebellum*. https://doi.org/10.1007/s12311-023-01575-9

Badaloni, A., Casoni, F., Croci, L., Chiara, F., Bizzoca, A., Gennarini, G. et al. (2019) Dynamic expression and new functions of early B cell factor 2 in cerebellar development. *Cerebellum*, 18, 999–1010.

Bagnall, M.W., Zingg, B., Sakatos, A., Moghadam, S.H., Zeilhofer, H.U. & du Lac, S. (2009) Glycinergic projection neurons of the cerebellum. *The Journal of Neuroscience*, 29, 10104–10110.

Casoni, F., Croci, L., Bosone, C., D'Ambrosio, R., Badaloni, A., Gaudesi, D. et al. (2017) Zfp423/ZNF423 regulates cell cycle progression, the mode of cell division and the DNA-damage response in Purkinje neuron progenitors. *Development*, 144, 3686–3697.

Casoni, F., Croci, L., Vincenti, F., Podini, P., Riba, M., Massimino, L. et al. (2020) ZFP423 regulates early patterning and multiciliogenesis in the hindbrain choroid plexus. *Development*, 147(22), dev190173.

Chen, S. & Hillman, D.E. (1993) Colocalization of neurotransmitters in the deep cerebellar nuclei. *Journal of Neurocytology*, 22, 81–91.

Chung, S.H., Marzban, H. & Hawkes, R. (2009) Compartmentation of the cerebellar nuclei of the mouse. *Neuroscience*, 161, 123–138.

Ekerot, C.F., Garwicz, M. & Schouenborg, J. (1991) The postsynaptic dorsal column pathway mediates cutaneous nociceptive information to cerebellar climbing fibres in the cat. *The Journal of Physiology*, 441, 275–284.

Fink, A.J., Englund, C., Daza, R.A., Pham, D., Lau, C., Nivison, M. et al. (2006) Development of the deep cerebellar nuclei: transcription factors and cell migration from the rhombic lip. *The Journal of Neuroscience*, 26, 3066–3076.

Flood, S. & Jansen, J. (1961) On the cerebellar nuclei in the cat. *Acta Anatomica (Basel)*, 46, 52–72.

Fujita, H., Kodama, T. & du Lac, S. (2020) Modular output circuits of the fastigial nucleus for diverse motor and nonmotor functions of the cerebellar vermis. *eLife*, 9, e58613.

Fujita, H., Oh-Nishi, A., Obayashi, S. & Sugihara, I. (2010) Organization of the marmoset cerebellum in three-dimensional space: lobulation, aldolase C compartmentalization and axonal projection. *The Journal of Comparative Neurology*, 518, 1764–1791.

Garwicz, M. & Ekerot, C.F. (1994) Topographical organization of the cerebellar cortical projection to nucleus interpositus anterior in the cat. *The Journal of Physiology*, 474, 245–260.

Gilthorpe, J.D., Papantoniou, E.K., Chedotal, A., Lumsden, A. & Wingate, R.J. (2002) The migration of cerebellar rhombic lip derivatives. *Development*, 129, 4719–4728.

Goodman, D.C., Hallett, R.E. & Welch, R.B. (1963) Patterns of localization in the cerebellar Corticonuclear projections of albino rat. *The Journal of Comparative Neurology*, 121, 51–67.

Green, M.J. & Wingate, R.J. (2014) Developmental origins of diversity in cerebellar output nuclei. *Neural Development*, 9, 1.

Hawkes, R. (2018) The Ferdinando Rossi memorial lecture: zones and stripes-pattern formation in the cerebellum. *Cerebellum*, 17, 12–16.

He, X., Treacy, M.N., Simmons, D.M., Ingraham, H.A., Swanson, L.W. & Rosenfeld, M.G. (1989) Expression of a large family of POU-domain regulatory genes in mammalian brain development. *Nature*, 340, 35–41.

Houck, B.D. & Person, A.L. (2015) Cerebellar premotor output neurons collateralize to innervate the cerebellar cortex. *The Journal of Comparative Neurology*, 523, 2254–2271.

Ikeda, M., Houtani, T., Nakagawa, H., Baba, K., Kondoh, A., Ueyama, T. et al. (1995) Enkephalin-immunoreactive fastigial neurons in the rat cerebellum project to upper cervical cord segments. *Brain Research*, 690, 225–230.

Kebschull, J.M., Casoni, F., Consalez, G.G., Goldowitz, D., Hawkes, R., Ruigrok, T.J.H. et al. (2023) Cerebellum lecture: the cerebellar nuclei-Core of the cerebellum. *Cerebellum*, 23, 620–677.

Kebschull, J.M., Richman, E.B., Ringach, N., Friedmann, D., Albarran, E., Kolluru, S.S. et al. (2020) Cerebellar nuclei evolved by repeatedly duplicating a conserved cell-type set. *Science*, 370, eabd5059.

Kebschull, J.M. & Zador, A.M. (2018) Cellular barcoding: lineage tracing, screening and beyond. *Nature Methods*, 15, 871–879.

Kim, C.K., Adhikari, A. & Deisseroth, K. (2017) Integration of optogenetics with complementary methodologies in systems neuroscience. *Nature Reviews. Neuroscience*, 18, 222–235.

Korneliussen, H.K. (1968) On the morphology and subdivision of the cerebellar nuclei of the rat. *Journal für Hirnforschung*, 10, 109–122.

Legue, E. & Joyner, A.L. (2010) Genetic fate mapping using site-specific recombinases. *Methods in Enzymology*, 477, 153–181.

Lugaro, E. (1895) Sulla struttura del nucleo dentato del cervelletto nell'uomo. *Monitore Zoologico Italiano*, 6, 5–12.

Machold, R. & Fishell, G. (2005) Math1 is expressed in temporally discrete pools of cerebellar rhombic-lip neural progenitors. *Neuron*, 48, 17–24.

Madisen, L., Zwingman, T.A., Sunkin, S.M., Oh, S.W., Zariwala, H.A., Gu, H. et al. (2010) A robust and high-throughput Cre reporting and characterization system for the whole mouse brain. *Nature Neuroscience*, 13, 133–140.

Morales, D. & Hatten, M.E. (2006) Molecular markers of neuronal progenitors in the embryonic cerebellar anlage. *The Journal of Neuroscience*, 26, 12226–12236.

Nakamura, T., Jenkins, N.A. & Copeland, N.G. (1996) Identification of a new family of Pbx-related homeobox genes. *Oncogene*, 13, 2235–2242.

Nectow, A.R. & Nestler, E.J. (2020) Viral tools for neuroscience. *Nature Reviews. Neuroscience*, 21, 669–681.

Ortiz, C., Carlen, M. & Meletis, K. (2021) Spatial Transcriptomics: molecular maps of the mammalian brain. *Annual Review of Neuroscience*, 44, 547–562.

Paxinos, G.W.C. (2007) *The rat brain in stereotaxic coordinates*. London: Academic Press.

Rao, A., Barkley, D., Franca, G.S. & Yanai, I. (2021) Exploring tissue architecture using spatial transcriptomics. *Nature*, 596, 211–220.

Uusisaari, M. & Knopfel, T. (2008) GABAergic synaptic communication in the GABAergic and non-GABAergic cells in the deep cerebellar nuclei. *Neuroscience*, 156, 537–549.

Uusisaari, M. & Knopfel, T. (2010) GlyT2+ neurons in the lateral cerebellar nucleus. *Cerebellum*, 9, 42–55.

Uusisaari, M. & Knopfel, T. (2011) Functional classification of neurons in the mouse lateral cerebellar nuclei. *Cerebellum*, 10, 637–646.

Wang, V.Y., Rose, M.F. & Zoghbi, H.Y. (2005) Math1 expression redefines the rhombic lip derivatives and reveals novel lineages within the brainstem and cerebellum. *Neuron*, 48, 31–43.

Weidenreich, F. (1899) Zur Anatomie der Centralen Kleinhirnkerne der Säuger. *Zeitschrift für Morphologie und L'Anthropologie*, Bd.1, H.2, p259–312.

White, J.J. & Sillitoe, R.V. (2017) Genetic silencing of olivocerebellar synapses causes dystonia-like behaviour in mice. *Nature Communications*, 8, 14912.

Willett, R.T., Bayin, N.S., Lee, A.S., Krishnamurthy, A., Wojcinski, A., Lao, Z. et al. (2019) Cerebellar nuclei excitatory neurons regulate developmental scaling of presynaptic Purkinje cell number and organ growth. *eLife*, 8, e50617.

Wingate, R. (2005) Math-map(ic)s. *Neuron*, 48, 1–4.

Wu, J.P.H., Yeung, J., Rahimi-Balaei, M., Wu, S.R., Zoghbi, H. & Goldowitz, D. (2022) The transcription factor Pou3f1 sheds light on the development and molecular diversity of glutamatergic cerebellar nuclear neurons in the mouse. *Frontiers in Molecular Neuroscience*, 15, 921901.